JOURNAL OF MATERIALS SCIENCE 17 (1982) 164–176

Biaxial impact fatigue of polycarbonate

M. T. TAKEMORI
Polymer Physics and Engineering Branch, Corporate Research and Development Center, General Electric Company, Schenectady, New York 12301, USA

An impact fatigue test has been designed for studying the repeated biaxial impact load response of polymers. In the test geometry, a thin plate-like sample is rigidly held by an annular clamp and is repeatedly impacted by a hemispherically-tipped plunger. Results have been obtained for polycarbonate. Under impact fatigue, cracks initiate on the bottom surface where high biaxial tensile stresses exist. These cracks propagate along radial lines on the sample surface and also into the sample normal to the surface. The load-bearing capability and the residual impact strength decrease as the cracks propagate. The development of impact fatigue cracks, the lifetime behaviour and the change in mechanical properties after partial impact fatigue are discussed.

1. Introduction

The general mechanisms for strengthening and toughening polymers are reasonably well understood [1, 2]. It is therefore not surprising that polymers used in structural applications have excellent strength and impact resistance. However, it is also not surprising that other problems which are not presently being addressed in design considerations are becoming evident. One of these problems is fatigue. There is one aspect of fatigue damage which is often unrecognized: the fatigue-induced degradation of physical and mechanical properties as a result of partial fatigue. This degradation of mechanical properties can be of two types: (a) the partially-fatigued sample fails in the same fashion as in the unfatigued sample but at much lower stress levels, or (b) the partially-fatigued failure occurs in a different mode, the most outstanding case being that of a normally ductile polymer failing by brittle crack propagation.

In an effort to examine this effect more closely, an impact fatigue test of a sample held by an annular clamp and repeatedly impacted by a hemispherically-tipped plunger was designed. This test was chosen to study the effects of in-plane biaxial tensile stresses on plate-like samples, which are commonly found in many polymer applications. The stress state on the side opposite the loading is biaxial tension, which favours crack formation. Thus, fatigue cracks would preferentially initiate and grow on the side which is often not readily visible, for example, the inside surface of a housing (when the loading is on the exposed outer surface). The aim of the present study is to understand the damage mechanisms in this biaxial loading mode and the deleterious effects of impact fatigue on the mechanical properties.

There have been few reported studies on the impact fatigue response of polymers. Bhateja *et al.* [3] studied the response of ultra-high molecular weight linear polyethylene under low cycle (less than 20) repeated impacting of notched samples under three-point bending. Ohishi *et al.* [4] studied unnotched polycarbonate under a repeated dropped weight, three-point bending apparatus and mapped out a stress–number of cycles to failure (S/N) impact fatigue diagram. Schater *et al.* [5] studied the effect of repeated impact on polymer surfaces in terms of heat generation and mechanochemical reactions, while Studman and Field [6] examined the surface damage due to low velocity, angled impacts on polymethylmethacrylate. These last two investigations were basically concerned with wear resistance. Other efforts to understand the failure of machine parts and structural members have led to impact fatigue studies of metals (see, for example, [7, 8]). To the present author's knowledge, however, there has not been any detailed study of the biaxial impact-fatigue response of ductile polymers.

0022–2461/82/010164–13$03.30/0

2. Experimental procedure

The testing was performed on polycarbonate (PC) extruded sheet (0.32 cm thick) cut into samples of 10 cm x 10 cm. The impact fatigue tests were carried out on a Instron Model 1350 servo-hydraulic testing machine. The specimen clamping and loading arrangement is shown in Fig. 1. Each specimen was rigidly held by an annular clamp with an inner diameter of 4 cm. In this arrangement, the centre of the sample was repeatedly impacted by a hardened steel plunger with a hemispherically-shaped tip with a radius of curvature of 0.5 cm. For this experiment, the plunger was fixed while the specimen was displaced sinusoidally at 10 Hz with an amplitude of 0.178 cm. The displacement (stroke) was feed-back controlled and, hence, a constant maximum penetration was maintained on each impact cycle. The plunger contacted the sample during 25 to 40 per cent of the total cycle time, the exact duration depending upon the initial maximum load desired. The desired initial peak load was established by adjusting the mean relative distance between the plunger and the sample prior to fatigue testing. Each adjustment was made by changing the mean level of the stroke command signal of the Instron electronic control module and observing the peak load on a single cycle. Approximately 5 adjustements were required to obtain the desired peak load. After the desired load was obtained, the fatigue test was initiated. At specified intervals, the load and displacement signals were recorded on a Nicolet Corporation EXPLORER III digital storage oscilloscope and transferred to an on-line microcomputer which calculated (in real time) the peak load per cycle, the initial slope of the load–displacement curve (a measure of stiffness), energy input and energy loss per cycle. The surface temperature was monitored on selected samples using a Ni resistance thermometer which was secured directly opposite the loading zone.

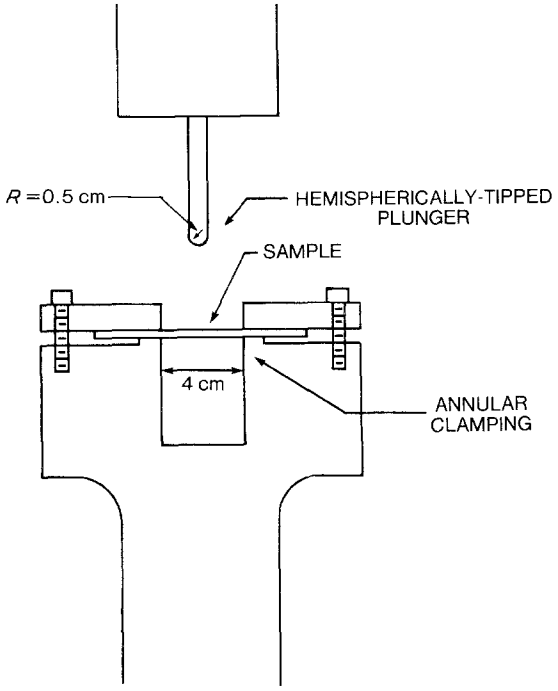

Figure 1 Sample clamping and loading geometry.

3. Results

3.1. Biaxial impact fatigue crack development

The initial cyclic peak loads chosen for this study are considerably less than the biaxial impact strength of the polycarbonate. Under the same experimental conditions described, i.e., for a 0.32 cm thick specimen using a 1 cm diameter plunger and a 4 cm diameter annular clamp, the peak load before failure (for a monotonic loading at a plunger speed of 25.4 cm sec^{-1}) is approximately 5300 N [9]. The biaxial impact fatigue tests reported here were obtained for initial maximum loads of between 267 and 623 N. At these lower load values, the dominant deformation mechanism is fatigue crack formation and propagation. At high initial peak loads (greater than 623 N) the nature of the impact fatigue damage process is drastically different: the dominant deformation mechanism is bulk yielding, rather than crack formation, and is accompanied by significant heating. The high initial peak load data will not be discussed further in this paper.

Fig. 2 presents the impact-fatigue lifetime data for the polycarbonate. For the purposes of this test, the impact-fatigue lifetime was chosen to be the number of cycles until the appearance of a large crack. Experimentally this is easily determined by monitoring the peak load per cycle. The appearance of a large crack precipitates a drastic lowering of the cyclic peak load, as shown in Fig. 3. There appears to be an endurance limit below 267 N, but at high initial cyclic peak loads, a very rapid decrease in impact fatigue lifetime can be seen.

For the lower initial peak load tests, the biaxial impact fatigue deformation process can be separated into three distinct phases. In the first phase

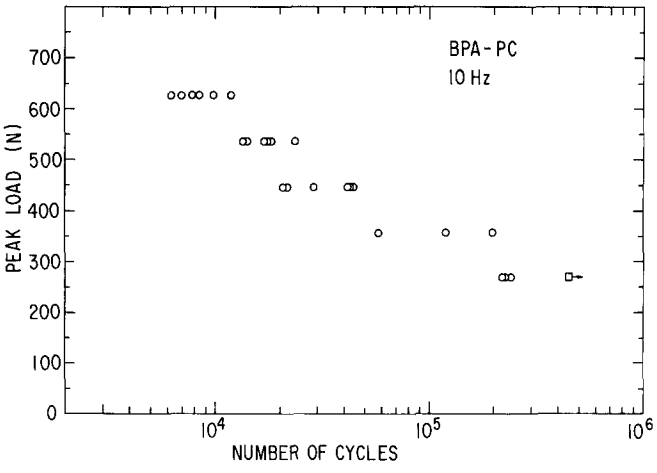

Figure 2 Impact fatigue lifetimes. Failure was determined by the appearance of a "fatal" crack. The sample denoted by a square did not fail.

the cyclic peak load drops as the plunger tip penetrates the top surface of the specimen at the contact point. In the next phase, the peak load levels off and small cracks nucleate and grow on the bottom surface directly opposite the plunger contact area. These cracks grow in two distinct regions, the centre, and an annular region around the centre. In the final phase, the peak load drops dramatically as a large multi-branched radial crack propagates across the bottom of the sample. The crack initially grows rapidly but, as the crack tips get further away from the centre, the crack enters reduced-stress zones and the crack growth rate is lowered. The peak load again remains relatively constant, but at a much reduced value since the large crack significantly reduces the stiffness of the sample. In Fig. 3, the peak-load results for typical fatigue tests clearly show these three phases. The impact-fatigue lifetime, chosen for the lifetime data shown in Fig. 2, corresponds to the onset of large cracks and was determined by the sharp drop in peak load at the beginning of the third phase. A more detailed description of the three phases follows.

3.1.1. First phase: penetration

The early decrease in the peak load for each cycle is due to penetration of the sample by the plunger tip on the loading surface (top surface of Fig. 1). Since the relative displacement of the plunger (stroke) is controlled, the penetration of the sample would lead to a corresponding decrease in the peak load experienced by the sample at the maximum stroke position. This decrease can be estimated by the elastic–plastic model described in the Appendix. Assuming that the penetrated

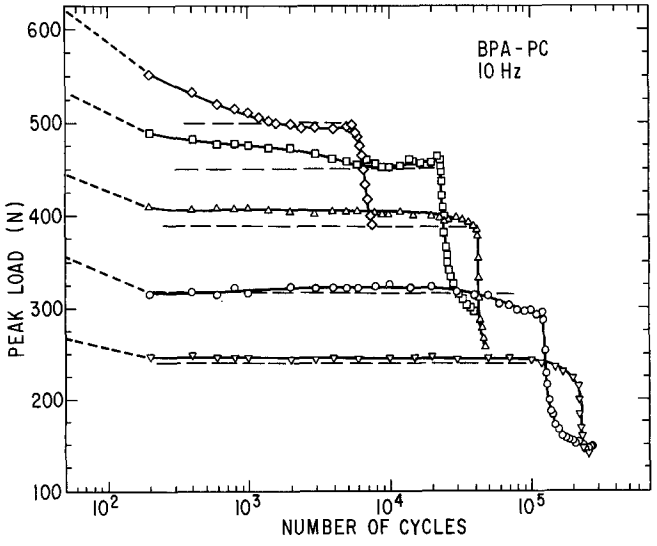

Figure 3 Typical peak load curves for five different samples. Horizontal dashed lines are the peak load values predicted by the simple penetration model discussed in the text.

TABLE I Reduced load maximum due to penetration

Initial peak load, F_0	Diameter of penetrated zone (cm)	Penetration depth, P (cm) ($R = 0.5$ cm)	Total deflection during impact (cm)	Theoretical reduced load maximum $F = F_0 - \Delta F$ (N)	Measured reduced load maximum, F' (N)
623	0.31	0.025	0.128	498	500 ± 15
534	0.26	0.017	0.109	449	465 ± 15
445	0.215	0.012	0.090	387	405 ± 15
356	0.18	0.008	0.072	316	320 ± 20
267	0.15	0.006	0.056	240	240 ± 15

region has the shape of the tip of the hemispherical plunger, the penetration depth, P, will then be given by

$$P = R\left\{1 - \left[1 - \left(\frac{K}{R}\right)^2\right]^{1/2}\right\}, \qquad (1)$$

where R is the radius of curvature of the plunger tip and K is the radius of the penetrated region, which can be directly measured. Assuming linearity in the force–deflection response of the bending plate (treating the plate as an elastic diaphragm), the load reduction ΔF is given by

$$\frac{\Delta F}{F_0} = \frac{P}{D},$$

where D is the total initial plate deflection (before penetration occurs) and F_0 is the initial load maximum. The calculated load drops are tabulated in Table I and are also shown as dashed lines in Fig. 3. Good agreement can be seen in all cases.

3.1.2. Second phase: small crack development

During the second phase, small fatigue cracks nucleate and grow on the bottom (tensile) surface opposite the loading. These cracks do not affect the load-bearing capability of the polymer (the cyclic peak load remaining relatively constant) nor do they adversely affect the ultimate impact strength of the polymer (as will be shown later). Fig. 4 shows a sequence of photographs showing the development of these cracks under an initial cyclic peak load of 445 N. Cracks appear to nucleate from two types of microscopic surface defects, both types probably arising from the extrusion process. The first type of surface defects are parallel surface texture markings which are spaced roughly 0.3 mm apart and which run transverse to the extrusion direction. (This surface texture can vary from sheet to sheet so all test results are reported on samples cut from the same sheet). The second type of defects are circular in shape and appear randomly across the sample. Although both parallel texture markings and circular defects are initially visible, these defects become visually more pronounced upon impact fatigue loading. This effect is clearly apparent in Fig. 4a and b. Fig. 5 shows a sequence of higher magnification photographs of a region of the surface containing both a circular defect and the parallel surface markings. Surface cracks can be seen to nucleate and grow at both types of defect sites.

Two distinct regions of crack development can be seen in Fig. 4, one being the central region and the other, annular region around the centre. Cracks nucleate first in the annular region. The uniform-load elastic plate-bending model presented in the Appendix can be used to calculate the stress field in this annular region. Assuming a uniform load (see Fig. 6 and Table I), given by the measured reduced load maximum, F', a load radius equal to the radius of the measured penetration zone, K, and Poisson's ratio of 0.42 [10], the radial and tangential stress distribution can be calculated. Fig. 6 schematically shows the stresses along a diameter. The calculated biaxial stress values in the annular region where the cracks initiate ($r \sim r_0$) and in the centre ($r = 0$) are tabulated in Table II. In the annular region the tangential stress exceeds the corresponding radial stress. Therefore, radial cracks (which are oriented normal to the maximum principle stress direction) are preferred to tangential cracks. The tangential stresses are plotted in Fig. 7.

For the high initial peak loads (445 to 623 N), the tangential stress at $r \sim r_0$ is approximately 79 MPa and the radial stresses are a few per cent lower. These calculated biaxial stress levels are somewhat greater than the uniaxial yield stress of polycarbonate, which is 66 MPa at a strain rate of 1.0 sec^{-1} [11]. The higher crack-initiation stress levels are most likely due to the residual compressive stresses found on the surface of extruded

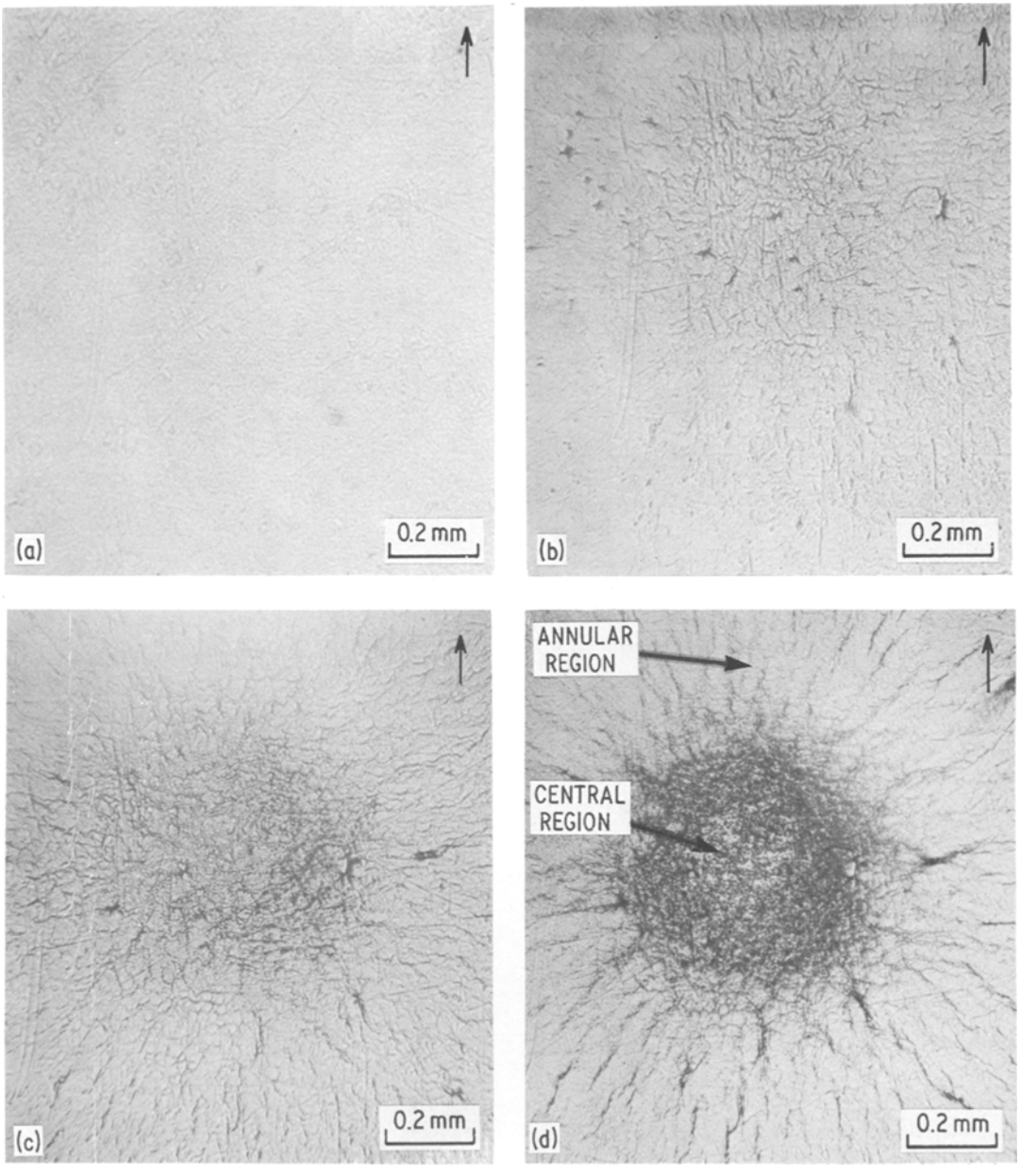

Figure 4 Sequential photographs of bottom surface opposite loading after (a) 0, (b) 2000, (c) 4000 and (d) 10 000 cycles. The initial peak load is 445 N. Two distinct regions of crack development can be seen. The small arrow in each micrograph indicates the extrusion direction.

sheets [12, 13]. Given the simplifying assumptions of a uniform load model, i.e., isotropy and ideal elastic plate bending, the agreement is quite reasonable. For these high initial peak load samples, a large number of radial cracks initiate and an annular corona of cracks develops. The growth of this corona is evident in Fig. 4.

For the two lower initial peak loads (267 and 356 N), the calculated stresses do not attain the biaxial stress level (79 MPa) which is necessary to generate a corona of radial cracks on the extruded sheet samples (see Table II and Fig. 7). On the other hand, isolated cracks initiate randomly at stress concentration sites (defects) located within or near the high-stress central region of the sample. Many repeated impacts are required for crack

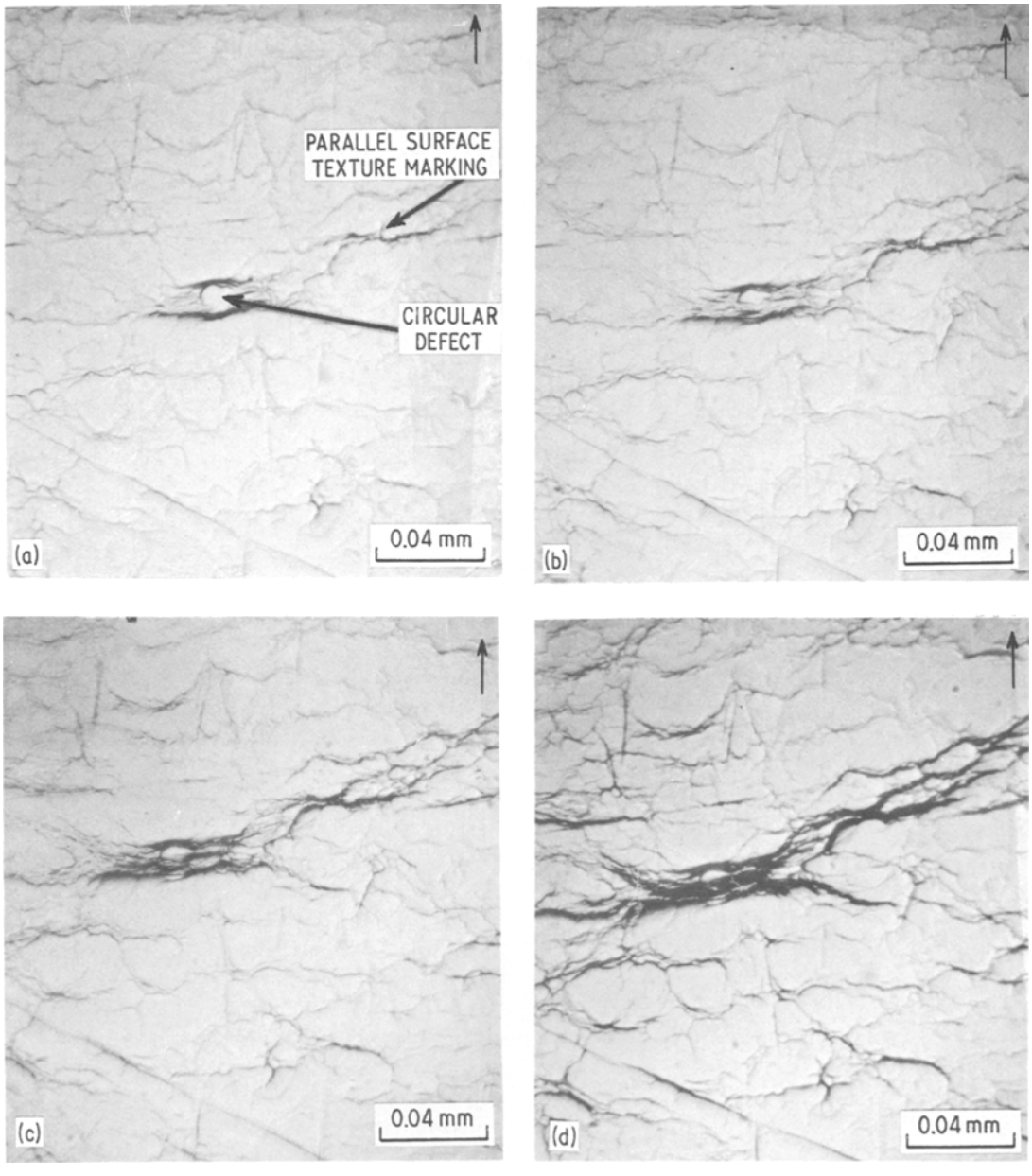

Figure 5 Higher magnification sequence of a portion of the right-hand side of Fig. 4 (in the annular region) showing the initiation of early cracks at two types of defect sites after (a) 4000, (b) 6000, (c) 10 000 and (d) 15 000 cycles. The crack propagation direction is along a radius. The small arrow in each micrograph indicates the extrusion direction.

nucleation and only a single or a few isolated radial cracks develop.

In uniaxial tensile fatigue tests [14, 15], as well as in four-point bend fatigue tests of polycarbonate [16], fatigue cracks initiate from surface crazes (which are oriented normal to the tensile loading direction). These crazes grow in length along the free surface and in depth into the specimen in a semi-elliptical shape. A surface view of such a craze grown under uniaxial tensile fatigue loading (4.5 to 45 MPa) can be seen in Fig. 8a. The surface growth is terminated by the formation of a pair of shear bands at each end of the craze opening. The free surface length of the "mature"

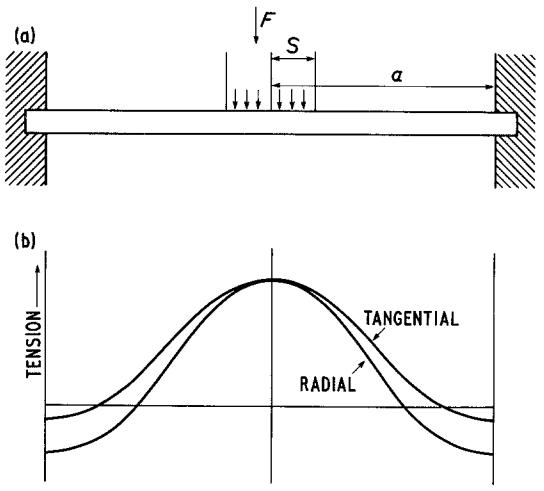

Figure 6 (a) The uniform load model, a uniform circular load (radius S) and circular opening (radius a). (b) Stress profile (along a diameter) on the bottom surface of sample. The stresses change sign along radii. Uniform biaxial tension exists at the centre.

craze is an inverse function of the applied stress as well as of the craze density [16], i.e., at higher applied loads (where the craze density is high), the free surface craze length is shorter than at low applied loads (low craze density). A crack subsequently develops within the craze and propagates along the entire crack front (radial and inward).

For the biaxial impact fatigue tests, crazes develop first, similar to the tensile and bending tests. Fig. 8b shows a biaxial impact fatigue crack-initiation site for an isolated surface crack under a low initial peak load (267 N) which nucleated at $r \sim 0.05$ cm, where the calculated σ_θ-value was 49 MPa ($\sigma_r = 48$ MPa). The "mature" craze length (assuming a craze initiated the crack) is indicated by the spacing between the shear-band initiation sites (approximately 50 μm). Fig. 8c shows an isolated surface crack ($r \sim 0.19$ cm) under a higher initial peak load (445 N) and calculated σ_θ-value of 45 MPa ($\sigma_r = 28$ MPa). A much shorter "mature" craze length of 20 μm can be seen. Both of these cracks initiated in a region of low craze density. Cracks nucleating in the annular corona, however, grow in a region of high craze density and, hence, the "mature" craze length is considerably shortened. Fig. 8d shows a typical radial surface craze/crack at $r \sim 0.09$ cm under a high initial peak load of 534 N and calculated σ_θ-value of 79 MPa ($\sigma_r = 76$ MPa). In all cases (Fig. 8a to d), surface shear bands radiate from the free surface ends of the "mature" craze.

The second distinct region of crack growth is the central region, where the uniform-load elastic plate-bending model presented in the Appendix predicts a uniform biaxial stress state. Fig. 9 shows an enlargement of the central region of the same sample shown in Fig. 4. A network of cracks is seen. There is strong evidence that these central cracks orient preferentially parallel with and perpendicular to the extrusion direction. These central cracks are only observed for the high initial peak loadings (445 to 623 N) where the calculated central stresses exceed 78 MPa. They are not observed for the low initial peak loadings, where the central stresses are 66 MPa and lower.

3.1.3. Third phase: large (fatal) crack development

In this third phase of the biaxial impact fatigue process, a large fatal crack grows rapidly (fatal because the load bearing capability decreases significantly). Despite the higher density of cracks within the annular region, the large fatal crack often grows just outside of the annular region. Fig. 10 shows the development of a fatal crack which initiated outside of the annular region and propagated radially. The many free-surface shear bands emanating from the initiation site form an

TABLE II Surface stresses

Initial peak load, F_0 (N)	Stress at centre* $\sigma_r(0) = \sigma_\theta(0)$ (MPa)	Measured radial distance to corona, r_0 (cm)	Stress at r_0	
			Radial, $\sigma_r(r_0)$ (MPa)	Tangential, $\sigma_\theta(r_0)$ (MPa)
623	85	0.10	76	79
534	84	0.08	77	80
445	78	0.04	76	77
356	66	No corona, isolated cracks		
267	52	No corona, isolated cracks		

*$\sigma_r(r)$ and $\sigma_\theta(r)$ are the surface stresses on the bottom (tensile) surface calculated from Equation A1 and A2. At the centre, $r = 0$.

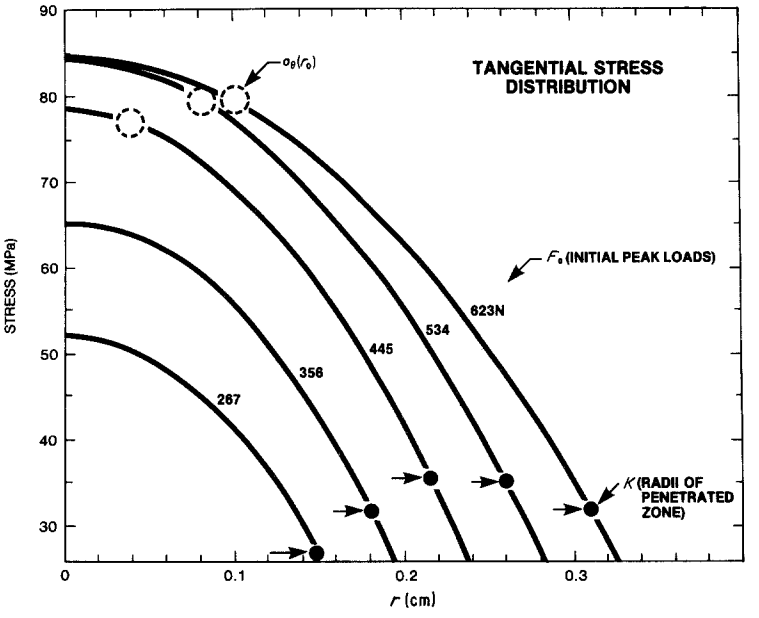

Figure 7 Tangential stress distribution calculated from the model in the Appendix. The measured reduced load maximum, F', and the measured penetration zone radius, K, (taken from Table I) are used. $\sigma_\theta(r_0)$ is the tangential stress at the annular crack initiation site (r_0). The two low initial load cases did not exhibit an annular corona of cracks. K is the radius of the penetration zone on the loading surface.

hour-glass pattern. The crack intersection with the free surface can be seen running through the sheared region on either side of the initiation site. The large crack rapidly grows through the centre and forms several radial branches. If only two branches grow, they are generally co-linear and equal in length, as expected by symmetry. When three branches form, one branch is often larger with two symmetrically-placed shorter branches on the opposite side of the centre. These branches

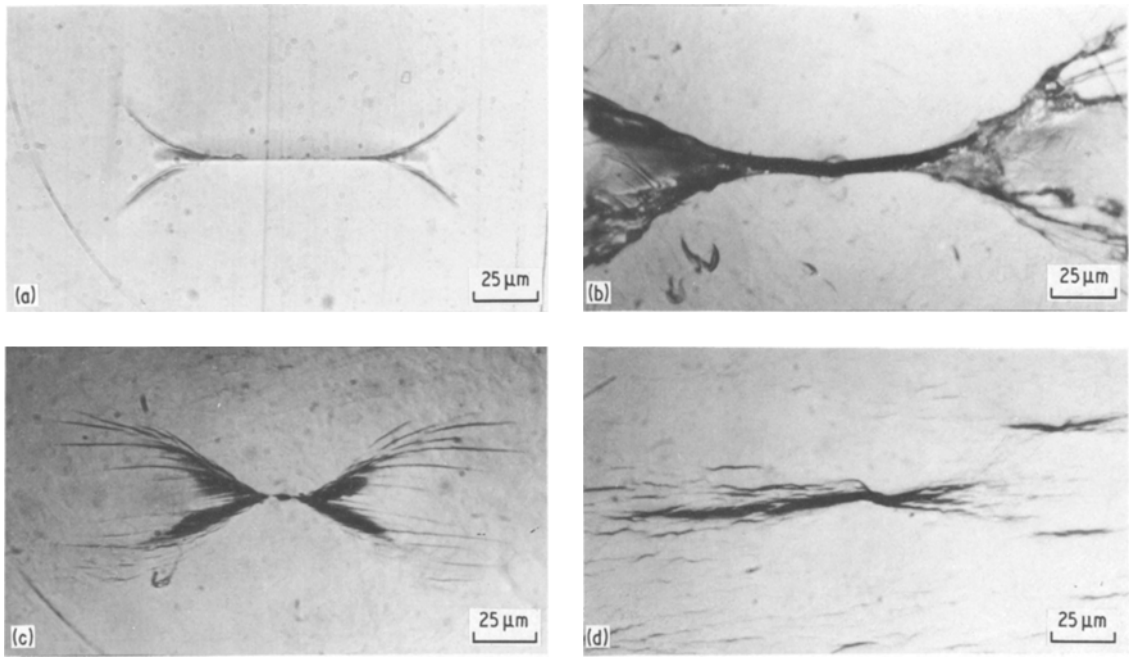

Figure 8 Surface photographs of craze/crack initiation sites, grown (a) under uniaxial tensile fatigue (45 MPa), (b) under biaxial impact fatigue (49 MPa) with low initial peak load (267 N), (c) under biaxial impact fatigue (45 MPa) with high initial peak load (445 N) and (d) in the annular corona of the crack (biaxial, 79 MPa). The maximum applied stresses are given in parentheses.

Figure 9 High-magnification photograph of the central region of Fig. 4 after 23 000 impacts showing the network-line structure of the central cracks. The small arrow indicates the extrusion direction.

grow rapidly until the crack tips enter the lower stress region away from the centre whereupon the crack growth-rate decreases sharply. At this point the peak load encountered on each cycle remains relatively constant at a much reduced level, the cracks make the sample a much more compliant diaphragm. There does not appear to be a preferred direction for this large crack growth.

A view of the crack fracture surface is shown in Fig. 11a. The shear bands near the free surface on either side of the initiation site show evidence of considerable yielding and tearing, indicating shear band formation and subsequent crack growth through the sheared region. Single cycle striations (Fig. 11b) as well as coarse bands (Fig. 11c) are often visible. Similar crack arrest features are seen under uniaxial tensile fatigue loading [14, 15].

3.2. Fatigue induced change in impact strength

In order to assess the effects of impact fatigue on mechanical properties, the residual impact strength was measured on partially impact-fatigued specimens. The impact strength was measured in the puncture mode using the same puncture fixtures of Fig. 1 in an MTS systems Corp. servohydraulic testing machine at a plunger rate of 25.4 cm sec^{-1}. Alignment holes in the specimen were used to ensure that the puncture occurred at the same spot as the prior impact fatigue loading. The total energy required to puncture the specimen, the peak load applied and the deflection at the peak load were measured. Fig. 12 shows some typical results. The uppermost curve shows the cyclic peak load curve during an impact fatigue test. A major "fatal" crack developed at roughly 30 000 cycles and caused a rapid drop in peak load. The bottom two curves of Fig. 12 show the puncture impact test results on partially-fatigued samples. There is essentially no change in the residual impact strength throughout the first two phases of the impact fatigue crack-growth process (i.e., up to 30 000 cycles) despite the growth of small fatigue cracks. In the third phase of the impact fatigue process of polycarbonate, however, when a large crack has formed, both the puncture impact strength and the peak load fall catastrophically. The puncture failure deformation mode also changes, as seen in the inset photographs of Fig. 12. Samples which have not been fatigued beyond the first two phases exhibit considerable yielding before fracturing in a circular path about the plunger. Towards the end of the second phase, a double (or multiple) hinged failure often occurs, with the fracture running through the centre cracks. Little reduction in impact strength results, however, as considerable yielding still occurs. In the third phase, the fracture mode changes sharply as the large crack extends rapidly, thereby accommodating most of the deflection with decreased yielding and energy absorption.

4. Conclusions

The biaxial impact fatigue loading configuration was chosen to model a commonly-found loading mode, i.e., biaxial planar stresses under repeated impacts. In extruded sheet polycarbonate, normally a ductile polymer, many small cracks initiate on the surface opposite the plunger loading surface at defects sites which are either small circular defects (pits) or texture markings which run in a transverse direction to the extrusion direction. These cracks grow in two regions: radials cracks in an annular region around the centre and randomly-oriented cracks in the centre. These radial and central cracks remain small for a considerable number of cycles. During this period the residual puncture impact properties remain constant. A

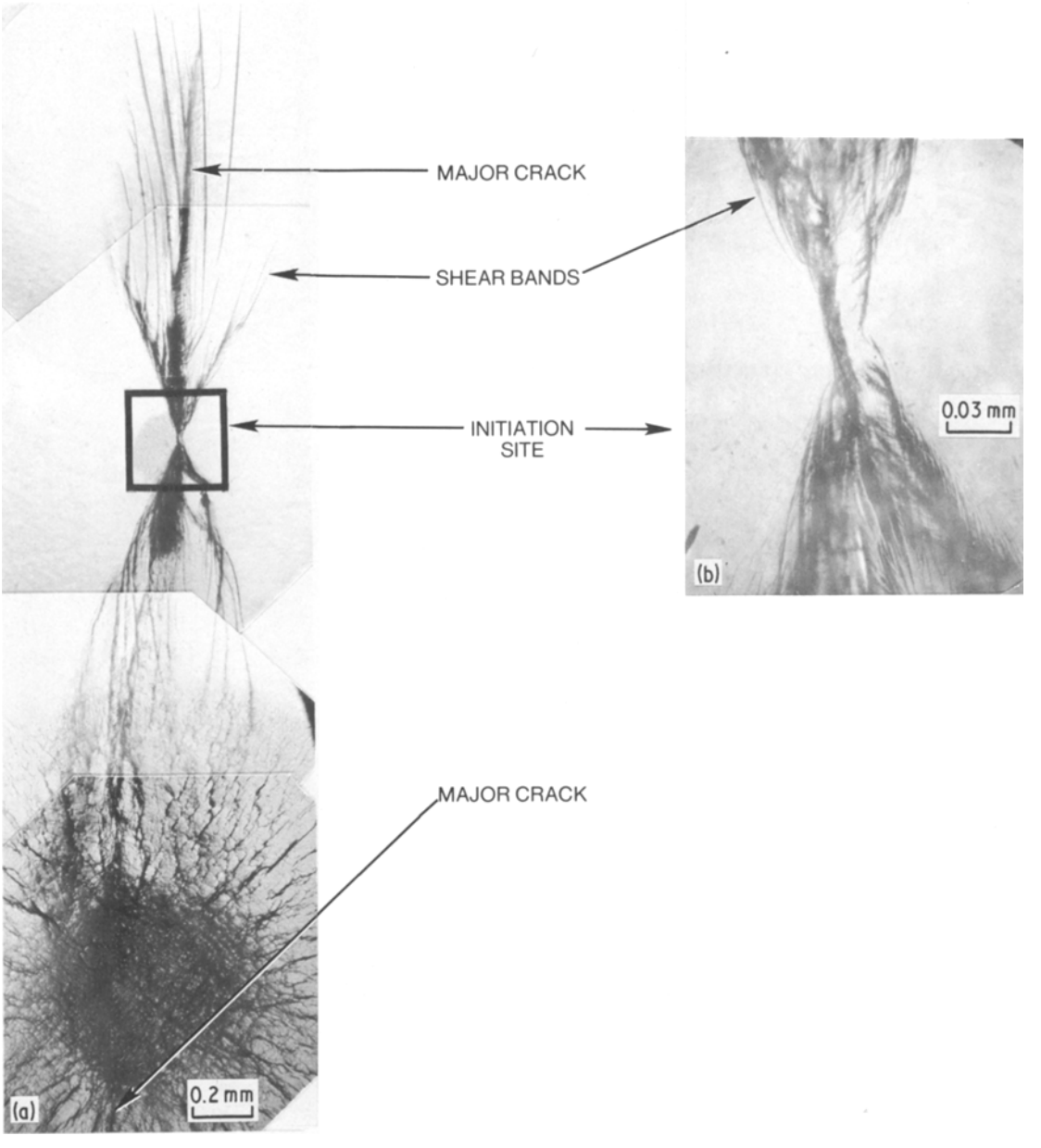

Figure 10 The growth of the "fatal" crack (after 23 170 impacts) for the sample shown in Fig. 4. The crack initiated outside the annular corona of cracks and propagated through the central region and away from the centre along a radius. (The major crack also propagated down into the specimen normal to the plane of the photograph. The crack has an elliptical shape with well-defined fatigue striations and a leading craze.)

large crack eventually initiates, often from a defect outside of the annular corona of radial cracks. The crack grows rapidly through the centre and forms several large branches which grow away from the centre and into lower stress regions. Growth is thus quickly slowed down. Once this large crack appears, the residual impact properties decrease abruptly. Although considerable yielding still occurs, the large crack provides an easy path for low-energy fracture and significantly reduces the impact strength and other ultimate properties.

Preliminary tests on other normally ductile polymers or polymer blends, such as ABS, reveal similar behaviour under impact fatigue, i.e., repeated impact loading generates fatigue cracks which, when sufficiently large, adversely affect

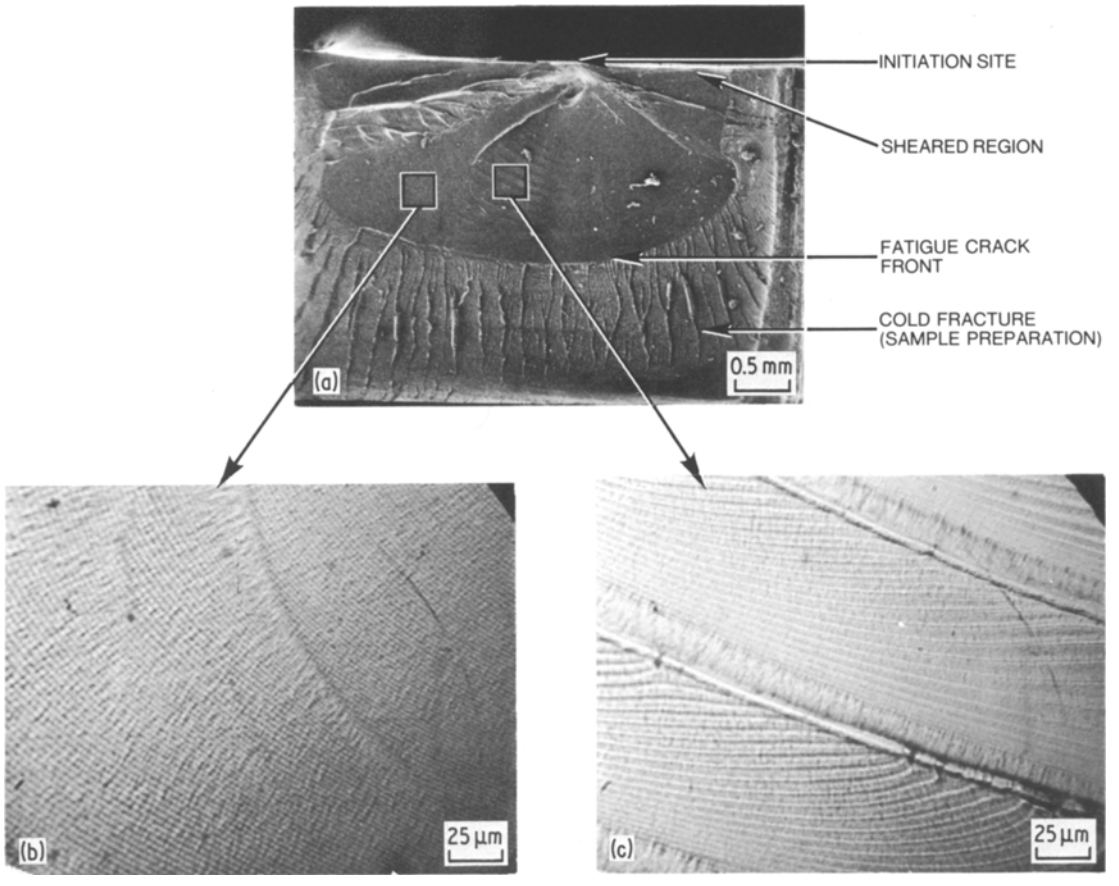

Figure 11 The impact fatigue-crack fracture surface: (a) overall view showing the semi-elliptical crack-front and the sheared region at the free surface; (b) single cycle fatigue striations; and (c) striations with coarse banding (see [14]).

the mechanical properties by altering the fracture mechanism from high-energy ductile flow to a lower energy mode with crack propagation and smaller scale yielding. The effects of conventional impact modification or toughening methods is also being examined. It appears that impact modification reduces fatigue crack-propagation rates, but at the expense of enhancing fatigue crack initiation. The net effect may be reduced fatigue properties. These observations will be reported in a later publication.

Acknowledgements

The author would like to thank Jay Moore for providing the polycarbonate extruded sheet and to Dean Matsumoto, Roger Kambour and Thomas Morelli for their helpful advice.

Appendix

In this appendix a mathematical model for the puncture process is presented. First, the elastic ideal plate-bending model for a uniform load is described and the handbook solutions for the stress state are presented. Then, an elastic-plastic model for the hemispherically-tipped plunger is presented.

A.1. Elastic ideal plate-bending: uniform load

As a starting point for our puncture model, the simple case of the ideal bending of a clamped circular specimen of uniform thickness, t, by a uniform circular load, F, is considered, see Fig. 6a. The surface stress distribution at radial distance, r, for an isotropic homogeneous sample (tensile modulus, E, and Poisson's ratio, ν) is given by [17] for $0 < r < S$:

$$\sigma_r(r) = \frac{3F}{2\pi t^2}\left[(1+\nu)\left(\ln\frac{S}{a} - \frac{S^2}{4a^2}\right) + (3+\nu)\frac{r^2}{4S^2}\right] \quad \text{(A1)}$$

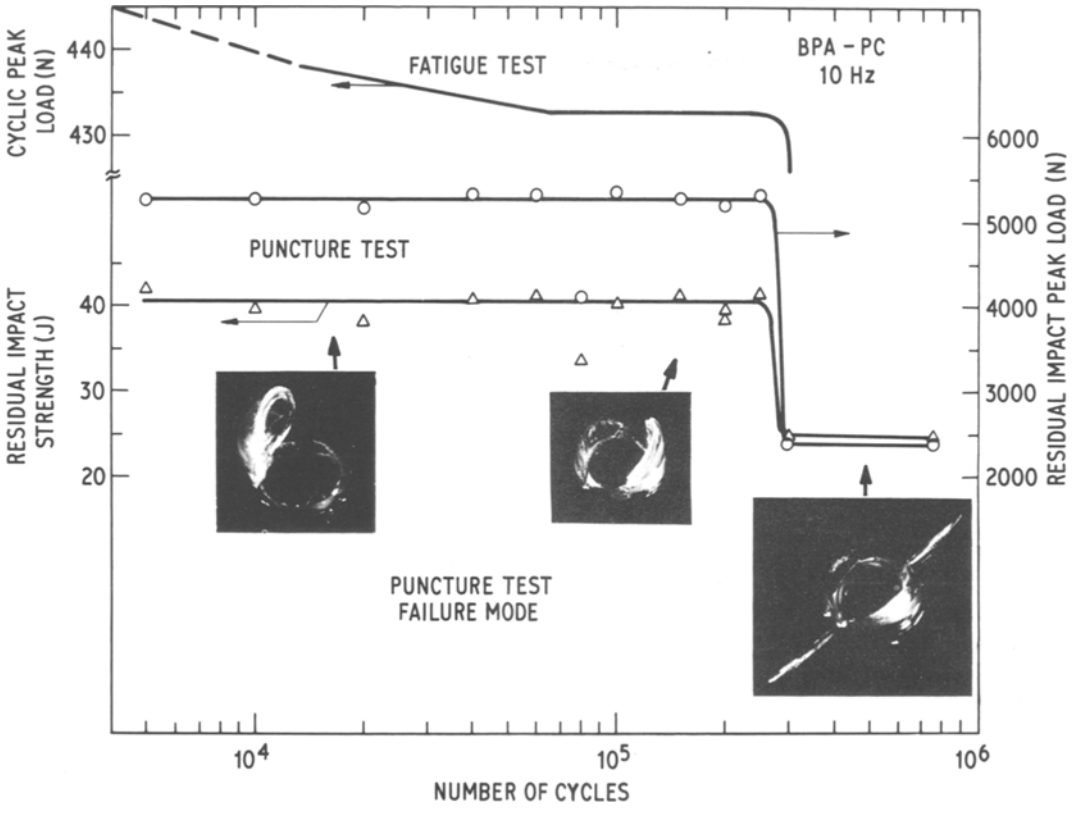

Figure 12 Two types of results are plotted. The uppermost curve shows a typical peak load curve observed during an impact fatigue test on a single specimen (similar to Fig. 3). The bottom two curves show the results of impact tests taken on many different specimens, each partially fatigued to a different number of impacts. The sharp drop in impact properties correlates well with the drop in peak load observed in a fatigue test. The insert photographs show typical failure modes for the partially-fatigued specimens that were subsequently punctured to failure.

and

$$\sigma_\theta(r) = \frac{3F}{2\pi t^2}\left[(1+\nu)\left(\ln\frac{S}{a} - \frac{S^2}{4a^2}\right) + (1+3\nu)\frac{r^2}{4S^2}\right]; \tag{A2}$$

and for $S < r < a$:

$$\sigma_r(r) = \frac{3F}{2\pi t^2}\left[(1+\nu)\left(\ln\frac{r}{a} - \frac{S^2}{4a^2}\right) - (1-\nu)\frac{S^2}{4r^2} + 1\right] \tag{A3}$$

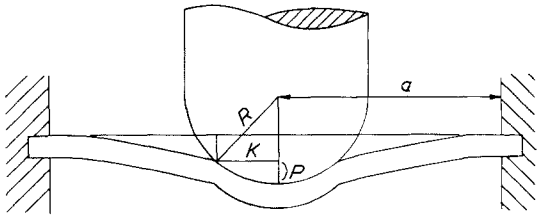

Figure 13 Hemispherically-tipped plunger geometry. P is the penetration depth.

and

$$\sigma_\theta(r) = \frac{3F}{2\pi t^2}\left[(1+\nu)\left(\ln\frac{r}{a} + \frac{S^2}{4a^2}\right) - (1-\nu)\frac{S^2}{4r^2} + \nu\right], \tag{A4}$$

where a is the plate radius, S is the load radius and σ_r and σ_θ refer to the radial and tangential stress components at the top (loading) surface. Under the assumption of ideal bending, the stress levels on the bottom surface are of the same magnitude but opposite sign and the stress varies linearly from top to bottom with a stress-free middle surface. Furthermore, the elastic limit is nowhere exceeded.

The vertical shear stress τ_z is given by

$$\tau_z = \frac{3F}{2\pi t^2}\frac{rt}{3S^2}, \qquad \text{for } 0 < r < S; \tag{A5}$$

and

$$\tau_z = \frac{3F}{2\pi t^2}\frac{t}{3r}, \qquad \text{for } S < r < a. \quad \text{(A6)}$$

The vertical shear stresses are generally small for thin plates and hence may be neglected. To a good approximation, the stress distribution is thus biaxial in the horizontal plane of the plate.

Fig. 6 shows the stress profile on the bottom surface for a plunger–hole diameter ratio, S/a, of 0.2. Due to the clamping geometry, the stresses change sign in going from the centre to the hole perimeter. The maximum stress state, which is uniform biaxial tension on the bottom surface and uniform biaxial compression on the top surface, is found at the centre of the circular samples. (This is found for the uniform load model as long as the plunger–hole diameter ratio does not exceed 0.588).

A.2. Elastic-plastic model: Hemispherically-tipped plunger

The geometry of the loading process is illustrated in Fig. 13, where a hemispherically-tipped plunger is shown. The hemispherical plunger penetrates the ductile polymer and the plunger–sample contact area is assumed to take the shape of the (undeformable) hemispherical plunger. The penetration depth of the plunger, P, is thus given by:

$$P = R\{1 - [1 - (K/R)^2]^{1/2}\}, \quad \text{(A7)}$$

where R is the radius of the hemispherical plunger tip and K is the radius of the penetrated central region.

References

1. C. B. BUCKNALL, "Toughened Plastics", (Applied Science Publishers Ltd, London, 1977).
2. I. M. WARD, "Mechanical Properties of Solid Polymers". (John Wiley and Sons, Chichester, 1971) p. 355.
3. S. K. BHATEJA, J. K. RIEKE and E. H. ANDREWS, *J. Mater. Sci.* **14** (1979) 2103.
4. F. OHISHI, S. NAKAMURA, D. KOYAMA, K. MINABE, Y. FUJISAWA and Y. TSURUGA, *J. Appl. Polymer Sci.* **20** (1976) 79.
5. E. SACHER, P. A. ENGEL and R. G. BAYER, *ibid.* **24** (1979) 1503.
6. C. J. STUDMAN and J. E. FIELD, *Wear* **41** (1977) 373.
7. H. IGUCHI, K. TANAKA and S. TAIRA, "Fatigue of Engineering Materials and Structures, Vol. 2 (Pergamon Press, Oxford, 1979). p. 165.
8. R. D. WELTZIN and G. KOVES, *J. Mater.* **3** (1968) 469.
9. G. R. TRYSON, M. T. TAKEMORI and A. F. YEE, 37th SPE ANTEC, Technical Papers, XXV, (Society of Plastics Engineers, 1979) 638.
10. M. T. TAKEMORI and A. F. YEE, unpublished work (1976).
11. A. F. YEE, *J. Mater. Sci.* **12** (1977) 757.
12. L. J. BROUTMAN and S. M. KRISHNAKUMAR, *Polymer Eng. Sci.* **16** (1976) 74.
13. J. R. SAFELL and A. H. WINDLE, *J. Appl. Polymer Sci.* **25** (1980) 1117.
14. M. E. MACKAY, T.-G. TENG and J. M. SCHULTZ, *J. Mater. Sci.* **14** (1979) 221.
15. M. T. TAKEMORI, unpublished work.
16. N. J. MILLS and N. WALKER, *J. Mater. Sci.* **15** (1980) 1832.
17. R. J. ROARK, "Formulas for Stress and Strain", 3rd Edn, (McGraw-Hill Book Co., New York, 1954).

Received 29 January
and accepted 18 June 1981